PRAMANA — journal of physics

Vol. 79, No. 5
November 2012
pp. 941–952

Recent neutrino oscillation results from T2K

H A TANAKA, on behalf of the T2K Collaboration
University of British Columbia and Institute of Particle Physics, Vancouver, BC, Canada V6T 1Z1
E-mail: tanaka@phas.ubc.ca

Abstract. The Tokai-to-Kamioka (T2K) experiment studies neutrino oscillations in a $\sim$ 600 MeV muon neutrino beam sent at 295 km from the Japan Proton Accelerator Complex (J-PARC) to the Super Kamiokande (SK) detector in Kamioka. The primary goals of T2K are to search for the appearance of electron neutrinos at SK resulting from $\theta_{13} > 0$ and to precisely measure θ_{23} and Δm^2_{32} via ν_μ disappearance. We report on T2K results obtained from neutrino data taken in 2010 and 2011.

Keywords. Neutrinos; weak interactions; CP violation.

PACS Nos 12.15.Ff; 14.60.Lm; 14.60.St; 14.60.Pq; 25.30.Pt

1. Introduction

Neutrino oscillations, in which neutrinos produced in one flavour interact with another flavour after propagating in space-time [1], were observed in solar [2] and atmospheric neutrinos [3], giving the first concrete evidence that neutrinos have non-zero and non-degenerate masses and undergo mixing between their mass and flavour eigenstates. These observations were confirmed by reactor and accelerator-based experiments [4,5] leading to a phase study where the parameters of the oscillations are being measured with increasing precision to elucidate the structure of neutrino mass and mixing, which is already known to be profoundly different from that observed in the quark sector [6].

In the 'standard' picture with three active neutrinos, the oscillations are governed by three mixing angles, namely, θ_{12}, θ_{13}, and θ_{23}, which parametrize the mixing matrix [1] that relates the mass eigenstates to the flavour eigenstates and govern the amplitudes of the oscillations, an irreducible CP-violating complex phase $\delta_{\rm CP}$, and three mass eigenvalues, whose squared differences Δm^2_{ij} determine the wavelengths of the oscillations in L/E, where L is the propagation distance and E is the energy of the neutrino. Conventionally, the θ_{12} mixing is attributed to the observed solar neutrino oscillations with $\Delta m^2_{21} \sim 7.8 \times 10^{-5}$ eV^2 and the θ_{23} mixing to the atmospheric neutrino oscillations with $\Delta m^2_{32} \sim 2.4 \times 10^{-3}$ eV^2.

Conclusive evidence for $\theta_{13} \neq 0$, which would lead to $\nu_\mu \rightarrow \nu_e$ appearance in accelerator-based ν_μ beams or $\bar{\nu}_e$ disappearance in reactor experiments at L/E

DOI: 10.1007/s12043-012-0411-5; ***e*Publication: 10 November 2012**

$\sim$500 km/GeV, has remained out of reach, with the MINOS and CHOOZ experiments setting limits on $\sin^2 2\theta_{13} < 0.12$ [7,8]. Since the other two mixing angles are known to be non-zero, the θ_{13} parameter is of particular interest as it endows the neutrinos with the full three-family mixing needed to induce CP-violation effects in neutrino oscillations, as conjectured by Kobayashi and Maskawa [9] in the quark sector. This CP violation would manifest itself in differences in the neutrino oscillation probabilities with their corresponding antineutrino channels and is of particular interest due to its possible connections to leptogenesis [10]. In addition, $\theta_{13} \neq 0$ will allow the possible determination of the mass hierarchy (i.e. the sign of Δm^2_{32}) through matter effects in the $\nu_\mu \rightarrow \nu_e$ oscillations. As a result, establishing $\theta_{13} \neq 0$ is a critical step towards studies of CP violation and matter effects resulting from the three flavour mixing. Current measurements of θ_{23} are consistent with the possibility that the mixing is maximal (i.e. $\theta_{23} = 45°$), leading to the speculation that some unknown symmetry may govern the neutrino mixing matrix. Thus, a precise measurement of θ_{23} is also of immense interest.

2. Experimental overview

The primary objectives of the Tokai-to-Kamioka (T2K) experiment are the search for $\nu_\mu \rightarrow \nu_e$ oscillations associated with $\theta_{13} \neq 0$ and the precise measurement of θ_{23}, Δm^2_{32} using the muon neutrino beam produced at J-PARC and detected 295 km away at the Super Kamiokande (SK) detector. Details of the experiment are given in [11] and a brief summary is provided here.

The neutrino beam for T2K is produced by 30 GeV protons from the J-PARC main ring. They are extracted in 8 bunches (6 in 2010) separated 581 ns apart and impinge upon a 91 cm long graphite target, resulting in the production of secondary particles. The target is embedded within a pulsed electromagnetic device ('horn') which produces a toroidal magnetic field that focusses positive secondary hadrons emerging from the target. The first horn is followed by two larger horns which provide additional focussing. Following the horns is a 90 m decay volume terminated by a beam dump in which the secondary particles, primarily π^+, decay to produce neutrinos. The target station and decay volume are filled with helium to minimize interactions and scattering of the outgoing hadrons. The beam dump terminates all particles apart from the neutrinos and high-energy muons. The latter are detected by a set of muon monitors (MuMon) situated behind the beam dump to measure the beam direction and rate stability on a spill-by-spill basis.

The T2K experiment uses the 'off-axis' beam configuration, which exploits a property of two-body decays where the energy of the decay products of pions at different momenta becomes lower and increasingly monoenergetic at angles away from the initial pion direction [12]. At T2K, the neutrino flux at the oscillation peak ($\sim$600 MeV at 295 km based on the measured value of Δm^2_{32}) is maximum at 2.5° from the axis of the beam. Hence the beam axis is directed 2.5° away from SK.

Figure 1 shows the history of T2K data-taking in 2010 and 2011 in terms of POT delivery, beam intensity (protons per pulse) and far detector data-taking efficiency. Totally, 1.43×10^{20} POT were delivered and usable for data analysis by 11 March 2011, when operations were interrupted by the 2011 Tohoku earthquake.

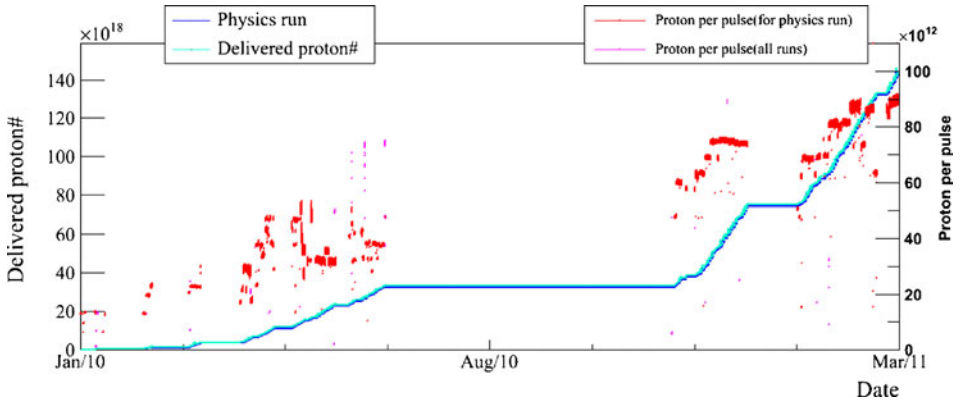

Figure 1. Summary of T2K proton delivery and data-taking efficiency in 2010–2011. The cyan line shows the integrated POT as a function of time, while the blue line shows the POT used in the analysis. The pink and red points show the per-pulse intensity for all the delivered beams and for data used in the analysis, respectively.

At 280 m from the target, there are two sets of neutrino detectors, one on-axis to the beam (INGRID) and the other off-axis in the direction of SK. The INGRID detectors are a set of 16 scintillator tracking detectors interspersed with iron for target mass that span the beam axis in both the horizontal and vertical directions, with two modules in diagonal positions. By measuring the yield of neutrino interaction per proton-on-target (POT) in each module, the beam centre can be measured with neutrino interactions on a daily basis. Based on the MuMon and INGRID measurements, the beam axis was found to be stable within 1 mrad during the 2010 and 2011 running periods as seen in figure 2.

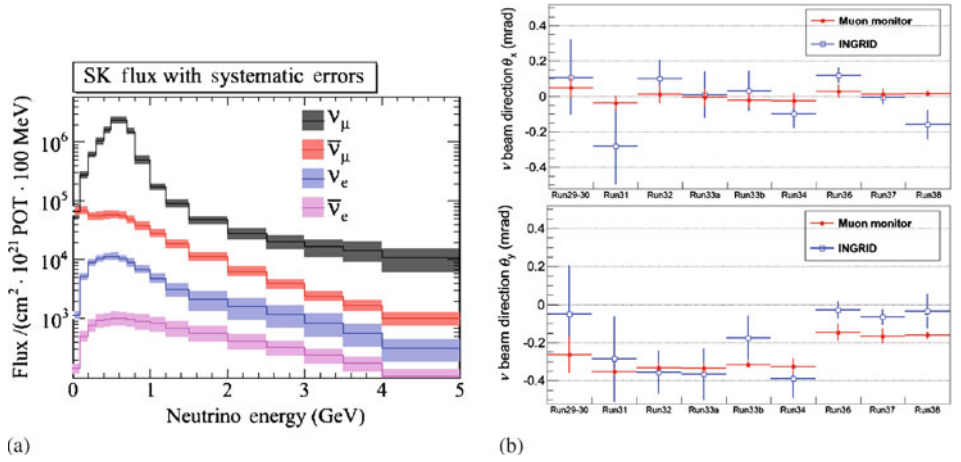

Figure 2. (**a**) The predicted neutrino flux at SK in the T2K beam. (**b**) MuMon and INGRID beam centre measurements as a function of time during the 2010–2011 data-taking period.

The off-axis detector comprises a magnetic tracking detector, a dedicated π^0 detector, an electromagnetic calorimeter, and muon range detectors. A 0.2 T magnetic field is provided by the refurbished UA1 magnet. The tracking detector consists of three large volume time projection chambers (TPCs) interspersed by two fine-grained scintillating tracking detectors (FGDs). The latter provides target mass and tracking at the neutrino interaction vertex, while the former provides sign and momentum information via the curvature in the magnetic field and particle identification through ionization loss measurements. The π^0 detector (P0D), which lies upstream of the tracking system, is a scintillating tracking detector with layers of brass and lead between the scintillator layers to enhance conversions of the decay photons. The FGDs and P0D contain water layers (removable in the latter case) to measure neutrino interaction properties on water.

The P0D and tracking detectors are surrounded by the ECAL, a lead/scintillator electromagnetic tracking calorimeter, that detects photons and provides further particle identification. Gaps in the UA1 magnet yoke are instrumented with large planes of scintillator (SMRD) to provide range measurement of muons produced at wide angles to the incident beam that penetrate through the ECAL and into the iron of the magnet.

The far detector is Super Kamiokande (SK), a 50 kt water Cherenkov detector instrumented with 11129 $20''$ photomultiplier tubes (PMTs). Data-taking is triggered via a GPS signal that opens a 1 ms gate in which the PMT activity around the expected neutrino arrival time is recorded. Neutrino interactions from the T2K beam are identified by the Cherenkov radiation produced by relativistic particles produced in the reaction, which result in ring patterns on the PMT array from which the particle vertex, direction, and energy can be determined. The topology of the ring can also allow the particle to be identified as muon- or electron-like. Multiparticle final states (such as that resulting from $\pi^0 \rightarrow \gamma + \gamma$) can be reconstructed by identifying rings corresponding to each particle.

3. Analysis overview

At T2K, the manifestation of $\nu_\mu \rightarrow \nu_e$ oscillations is an excess of ν_e interactions at the far detector over the expected background from misidentified interactions of other neutrino flavours and the intrinsic ν_e contamination in the beam. For the ν_μ disappearance, the oscillation parameters can be determined by the energy-dependent deficit of ν_μ interactions relative to the expectation without oscillations. At the T2K beam energy ($\mathcal{O}$(1 GeV)), the dominant charged current interaction channel is the quasielastic (CCQE) interaction: $\nu_\ell + n \rightarrow \ell^- + p$. This channel has an attractive feature that the neutrino energy can be reconstructed via the outgoing lepton momentum and angle relative to the (known) incident neutrino direction, and mostly has a simple, one-ring topology in the SK detector, since the recoil proton is usually produced below the Cherenkov threshold. Thus ν_e and ν_μ CCQE interactions at SK are the signal processes for the ν_e appearance and ν_μ disappearance analyses, respectively.

The backgrounds to the analysis in the absence of neutrino oscillations are obtained via a series of Monte Carlo (MC) simulations that starts with a neutrino flux determination, with which a comprehensive neutrino event generator [13] tuned to neutrino interaction and cross-section data (from previous experiments in the current analysis), determines

the expected neutrino interaction final states. These are then propagated through detailed detector simulations to determine the expected detector response and to assess selection efficiencies, reconstruction performance, and background rates.

The neutrino flux simulation is based on a detailed Geant3-based simulation [14], using FLUKA2008 [15] to simulate interactions in the carbon target. The optics of the primary proton beam based on the primary beam monitors and thin-target production data from NA61 are incorporated into the simulation [16]. The modelling of other hadronic interactions is tuned to relevant external cross-section measurements. Systematic uncertainties are obtained by varying the underlying source of uncertainty (e.g. off-axis angle, particle production cross-section, etc.) in the simulation and determining its effect on the predicted neutrino flux.

Due to the large *a priori* uncertainty in the flux and neutrino interaction predictions, the near detector is used to provide an overall rate normalization factor based on a ν_μ charged current (CC) inclusive sample. The predicted rates at the far detector are scaled by this measurement, allowing cancellations in the flux uncertainties. Since the extrapolation to other interaction channels of relevance (such as the neutral current π^0 production) from the ν_μ CC rate itself has large uncertainties and the cancellation in the neutrino interaction uncertainty is not significant with this method.

4. Near-detector measurements

The off-axis near detector (ND280) is used to select a sample of inclusive ν_μ CC interactions to provide an overall normalization factor for the event rate prediction in the far detector. The selection uses the tracker system (FGDs and TPCs) to identify interactions occurring in the FGD with a muon identified in the TPC. First, tracks are identified in the TPC and extrapolated into the FGD, where FGD hits along the projected path of a track are associated to it. These hits are used to define the starting point of the track. Among those tracks that start in the fiducial volume of the FGDs, the highest momentum negative track is required to be consistent with a muon using the $\mathrm{d}E/\mathrm{d}x$ measured in the TPC. The TPC upstream of the FGD is used as a veto to eliminate background from upstream interactions. With these requirements, 1529 ν_μ CC interactions are selected in the Run 1 data (2.88×10^{19} POT) with 38% efficiency and 90% purity. The yield is compared with the MC expectation to obtain a normalization factor:

$$R_{\mathrm{data/MC}} = 1.036 \pm 0.028(\mathrm{stat.})^{+0.044}_{-0.037}(\mathrm{det.\ sys.}) \pm 0.038(\mathrm{phys.\ mod.}), \quad (1)$$

which is used to scale the MC-predicted event rate expectations at the far detector. The systematic uncertainties of the detector are dominated by the modelling of the $\mathrm{d}E/\mathrm{d}x$ response of the TPC in the MC and track reconstruction efficiencies, which are studied using through-going muons in the neutrino and cosmic samples. The uncertainty of physics model includes neutrino interaction modelling uncertainties that affect the selection, such as the angular distribution of the primary muons and the hadronic final-state interactions. The uncertainty does not include flux prediction or neutrino cross-section errors that are expected to cancel the far detector rate prediction, with systematic uncertainties in the near/far extrapolation evaluated separately.

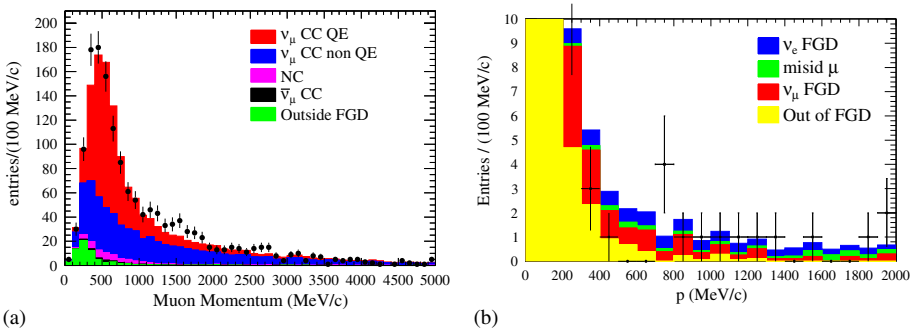

Figure 3. Reconstructed momentum distribution for ν_μ (**a**) and ν_e (**b**) charged current interactions in the ND280 FGD+TPC tracking system.

The reconstructed muon momentum (p_μ) of the selected events is shown in figure 3a. As a cross-check, the data/MC ratio is evaluated in two bins, $p_\mu < 2$ GeV/c and $p_\mu > 2$ GeV/c.

$$\begin{aligned} R_{<2\ \mathrm{GeV/c}} &= 1.041 \pm 0.029(\mathrm{stat.})^{+0.044}_{-0.054}(\mathrm{det.\ sys.}) \\ &\quad \pm 0.058(\mathrm{phys.\ mod.}), \\ R_{>2\ \mathrm{GeV/c}} &= 1.010 \pm 0.063(\mathrm{stat.})^{+0.047}_{-0.036}(\mathrm{det.\ sys.}) \\ &\quad \pm 0.046(\mathrm{phys.\ mod.}). \end{aligned} \tag{2}$$

The high momentum bin is particularly sensitive to ν_μ produced in $K_{\mu 2/3}$ decays of kaons in the beam, which have higher energy and comprise 74% of the events in this bin according to the MC. The K_{e3} decay modes of these kaons are the primary source of intrinsic ν_e background, and thus the consistency in the ν_μ channel gives confidence in the predicted ν_e background from kaon decay.

A further check on the ν_e background is provided by directly measuring the ν_e CC interaction rate in the ND280 tracker. In this case, the highest momentum track in the TPCs is identified and required to be negative and consistent with an electron by the measured $\mathrm{d}E/\mathrm{d}x$. Photon conversions are suppressed by pairing this track with other tracks in the event and events with a pair with invariant mass <100 MeV/c^2 are rejected. The momentum distribution of the 102 selected events in Run 1 (2.88×10^{19} POT) between 0 and 2 GeV/c, shown in figure 3b, is fit simultaneously with a sample of low momentum positive electron tracks and photon conversion candidates to constrain the photon conversion backgrounds and to extract the yield of ν_e CC events. The resulting double ratio $F = N_{\nu_e}/N_{\nu_\mu}$ between data and MC gives

$$F_{\mathrm{data}}/F_{\mathrm{MC}} = 0.6 \pm 0.4(\mathrm{stat.}) \pm 0.2(\mathrm{syst.}), \tag{3}$$

indicating that the MC-predicted rate of intrinsic ν_e interactions is consistent with the observed rate at ND280, albeit with large statistical uncertainty with the currently analysed ND280 data.

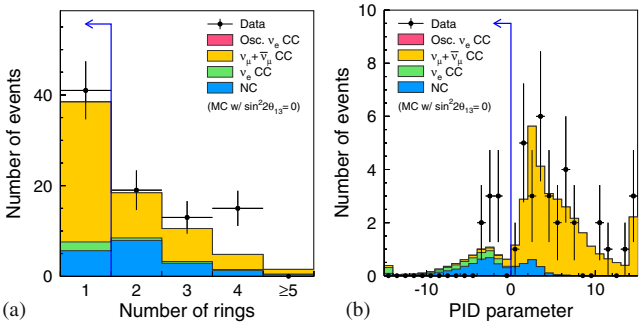

Figure 4. The number of rings identified (**a**) and the e/μ particle identification parameter (**b**) for FCFV events in the SK detector, where negative (positive) values are e-(μ)-like.

5. Far-detector event selection

The far-detector selection aims to identify ν_μ and ν_e CCQE events in the SK detector. The event selection starts by selecting fully-contained (FC) events with less than 16 hits in the outer detector and reconstructed vertex at least 2 m from the wall of the inner detector, resulting in a 22.5 kt fiducial volume (FV). Muon- and electron-induced Cherenkov rings can be distinguished topologically, with the more diffuse pattern for electrons arising from electromagnetic showering. Using the topology of the identified ring, namely the sharpness of the outer edge of the ring, the event can be further classified as ν_e or ν_μ CCQE based on whether the ring is electron- or muon-like.

For the ν_e CCQE selection, the dominant background comes in the form of intrinsic ν_e in the beam and NC π^0 events where a photon from the π^0 decay can mimic the electron signature if the other photon is undetected. For the ν_μ CCQE selection, the main background comes from pion production channels.

Table 1. Summary of the ν_μ CCQE selection at SK. The expectation assume $\Delta m^2_{32} = 2.4 \times 10^{-3}\,\mathrm{eV}^2$ and $\sin^2 2\theta_{23} = 1$. The last column shows the expected number of events in the absence of oscillations.

		Expected number of events				
Selection	Data	Total	ν_μ CCQE	ν_μ CCnQE	NC	w/o Osc.
FC+FV	88	74.1	19.0	33.8	18.3	166
Single ring	41	38.7	17.9	13.1	5.7	120
μ-like	33	32.0	17.6	12.4	1.9	112
$p_\nu > 200$ MeV/c	33	31.8	17.5	12.4	1.9	111
Decay $e \leq 1$	31	28.4	17.3	9.2	1.8	104

Table 2. Summary of the ν_e CCQE selection at SK. The expectation assumes ν_μ disappearence with $\Delta m^2_{32} = 2.4 \times 10^{-3}$ eV^2 and $\sin^2 2\theta_{23} = 1$, but $\theta_{13} = 0$. The last column shows the expected number of events from solar $\nu_\mu \rightarrow \nu_e$ oscillations, which is not included in the 'Total' column.

		Expected number of events for $\theta_{13} = 0$				
Selection	Data	Total	ν_μ CC	NC	ν_e CC	$\odot\ \nu_\mu \rightarrow \nu_e$
FC+FV	88	73.8	52.4	18.3	3.0	0.12
Single ring	41	38.4	30.9	5.7	1.9	0.11
e-like	8	6.7	1.0	3.7	1.9	0.11
$E_{\rm vis} > 100$ MeV	7	5.8	0.7	3.2	1.9	0.11
Decay $e = 0$	6	4.5	0.1	2.8	1.6	0.10
$M_{\rm inv} < 105$ MeV/c^2	6	1.9	0.04	0.8	1.1	0.09
$E_\nu^{\rm rec} < 1250$ MeV	6	1.4	0.03	0.6	0.8	0.09

Figure 4 illustrates this selection, with figure 4a showing the number of rings identified and figure 4b showing the particle identification parameter that distinguishes electrons and muons for single ring events. In the first stage, single ring events are selected to reject non-CCQE events. In the second stage, events are classified as e- or μ-like, resulting in the initial stages of the ν_e and ν_μ CCQE selection.

Additional information is available in the form of decay electrons arising from the $(\pi \rightarrow)\mu \rightarrow e$ decays of particles produced in the neutrino interaction, which can be identified as delayed activity in the event. CCQE events can be distinguished from non-CCQE events by the presence of decay electrons that may arise from pions produced in the event. In ν_μ CCQE interactions, the muon itself may give rise to a decay electron, hence we require that there is at most one decay electron. For ν_e CCQE events, no decay electrons are expected, and thus we require that the event has no identified decay electrons following the neutrino interactions.

For the ν_e CCQE selection, additional rejection of NC π^0 can be obtained by fitting candidate events to a two-ring hypothesis. By evaluating the invariant mass of the best-fit configuration, NC π^0 events with invariant mass consistent with the nominal π^0 mass that cannot be identified by the ring-counting technique can be suppressed. Finally, since the neutrino oscillation probability decreases at high energies, events with reconstructed neutrino energy $E_\nu^{\rm rec} > 1250$ MeV, where background from ν_e from kaon decay dominate, are rejected. Since we fit the $E_\nu^{\rm rec}$ distribution to extract the oscillation parameters in the ν_μ disappearance analysis, we do not employ this requirement in this case.

Tables 1 and 2 summarize the event selection for ν_μ and ν_e CCQE events, along with the corresponding expectations from the MC with near detector correction normalized to the 1.43×10^{20} POT. For table 1, the MC predictions include the effects of ν_μ disappearance with $\sin^2 2\theta = 1.0$ and $\Delta m^2 = 2.4 \times 10^{-3}$ eV^2. The last column shows the expected number of events in the absence of such oscillations. In table 2, the MC expectation is given with $\theta_{13} = 0$, with the last column giving the contribution from solar oscillations based on our current understanding of the oscillation parameters.

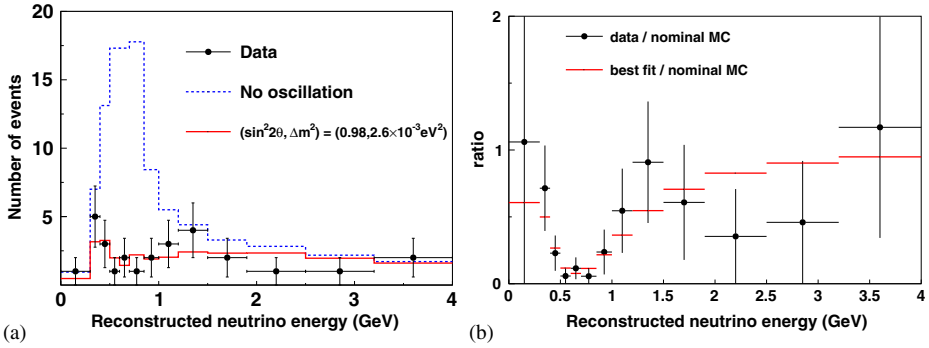

Figure 5. (**a**) Reconstructed neutrino energy distribution for ν_μ CCQE interactions identified at SK. (**b**) Ratio of the observed energy distribution to the expectation without oscillations.

6. ν_μ disappearance results

Figure 5a shows the $E_\nu^{\rm rec}$ distribution of the observed ν_μ CCQE candidates in the far detector. The histograms indicate the expected distribution in the absence of ν_μ disappearance effects (dashed blue line) and with the best-fit values of $\sin^2 2\theta_{23} = 0.99$ and $\Delta m^2_{32} = 2.6 \times 10^{-3}$ eV^2 (solid red line) resulting from a two-flavour analysis. A clear energy-dependent deficit consistent with ν_μ disappearance is observed, which is especially apparent when one takes the ratio of the observed $E_\nu^{\rm rec}$ distribution with the expectation in the absence of oscillations, as shown in figure 5b. Figure 7a shows the allowed regions extracted from the fit, where two fit methods were employed: one in which the systematic uncertainties are evaluated separately from the fit (dashed red line) and the other in which parameters governing these uncertainties are marginalized within the fit (solid red line). There are several leading categories of systematic uncertainties which include uncertainties in the non-CCQE background contribution, both in terms of the predicted rate and the reconstruction of these events, the modelling of the final-state interactions, uncertainties in the flux modelling and the near-detector normalization measurement. Altogether, this results in a $^{+15.0}_{-14.8}\%$ uncertainty in the expected event yield in the presence of oscillations with $\sin^2 2\theta_{23} = 1.0$ and $\Delta m^2_{32} = 2.4 \times 10^{-3}$ eV^2. Also shown are the allowed regions from recent analyses of SK atmospheric data and MINOS [17,18].

7. ν_e appearance results

The plots in figure 6 show the final stages of the ν_e selection in the far detector. Figure 6a shows the invariant mass distribution from the two-ring fit, where events with invariant mass >105 MeV/c^2 are rejected. In figure 6b, the $E_\nu^{\rm rec}$ distribution is shown; events in the background-dominated high-energy region $E_\nu^{\rm rec} > 1250$ MeV are rejected. Following this selection, six ν_e candidates remain with an expected background of 1.5 ± 0.3(sys.) events for $\theta_{13} = 0$. The systematic uncertainty in this error estimation includes contri-

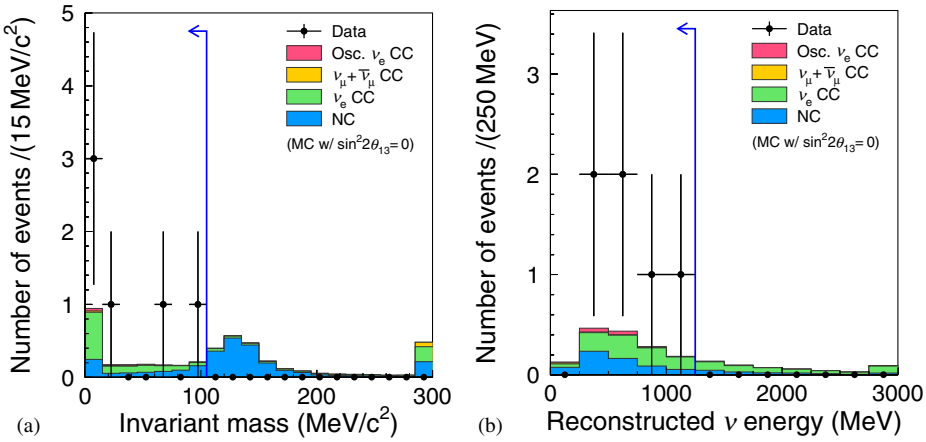

Figure 6. (**a**) The invariant mass distribution following the single-ring *e*-like selection and (**b**) the reconstructed neutrino energy distribution following the single-ring *e*-like, invariant mass distribution and decay electron selections.

butions from the flux (±8.5%), neutrino interaction modelling (±14.0%), near-detector normalization ($^{+5.6}_{-5.2}$%) and the SK detector response (±14.7%). The flux uncertainty is significantly reduced by the near-detector normalization, while the SK detector uncertainties associated with the selection are evaluated using control samples in the atmospheric neutrino data sample.

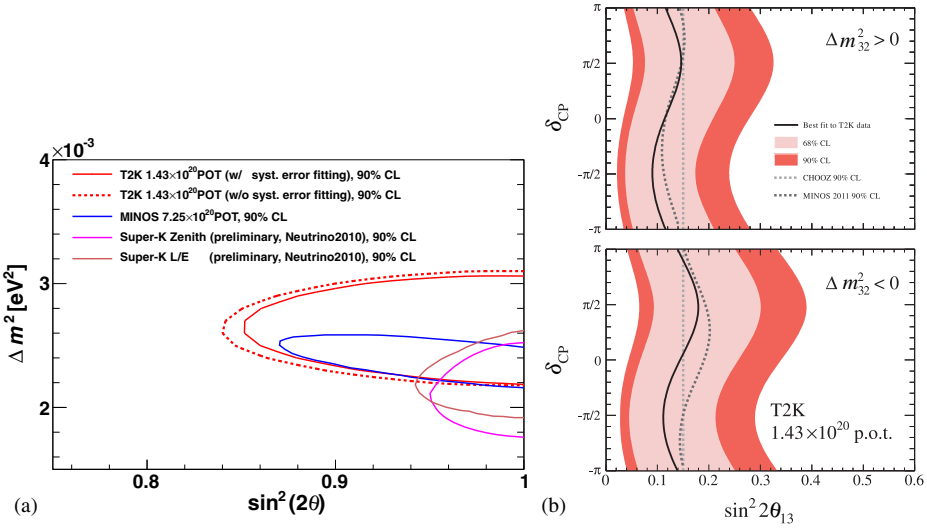

Figure 7. (**a**) Allowed regions in $\sin^2 2\theta_{23}$ and Δm^2_{32} from the ν_μ disappearance analysis. (**b**) Allowed regions in $\sin^2 2\theta_{13}$ as a function of $\delta_{\rm CP}$ from the ν_e appearance analysis for normal (top) and inverted (bottom) mass hierarchies.

For the ring counting and particle identification, the systematic uncertainties are extracted in a fit to various subcomponents of the atmospheric data, accounting for neutrino interaction uncertainties. For the π^0 specific cuts, the performance of the two-ring fit was assessed using a sample of 'hybrid' events where a single electron ring from the data was overlaid with an MC-generated ring in such a way that the kinematics are consistent with a π^0 decay. The first ring is selected from either the atmospheric neutrino sample (high-energy electron rings) or the decay electron sample (low energy). By comparing these data/MC hybrid events to those constructed from two MC-generated rings, discrepancies that arise from the mismodelling of the detector response due to the electromagnetic shower and optical photon propagation; and the PMT and electronics response can be probed, leading to an estimate of the systematic uncertainty.

Based on the estimated background in the case of the null hypothesis (i.e. $\theta_{13} = 0$), the P-value calculation for a fluctuation to six or more events is 0.7%. The allowed regions for θ_{13} as a function of the CP-violating phase $\delta_{\rm CP}$ for the two possible mass hierarchies are shown in figure 7b, together with a recent analysis of ν_e appearance oscillations from MINOS [19] and the CHOOZ experiment [7].

8. Conclusions

T2K has completed the analyses of $\nu_\mu \rightarrow \nu_e$ appearance [20] and ν_μ disappearance with data taken in 2010 and 2011, corresponding to 1.43×10^{20} protons-on-target and 2% of the final expectation for T2K. Six ν_e candidate events are observed on an expected background of 1.5 ± 0.3 events. The probability for the expected background to fluctuate for six or more events is 0.7%. The parameters θ_{23} and Δm^2_{32} are extracted from the ν_μ disappearance analysis with precision approaching the current best measurements from SK and MINOS. The experiment has recovered from the 11 March earthquake and plans to recommence operations at the beginning of 2012.

References

[1] B Pontecorvo, *JETP* **34**, 172 (1958)
Z Maki, M Nakagawa and S Sakata, *Prog. Theor. Phys.* **28**, 870 (1962)
[2] B T Cleveland *et al*, *Astrophys. J.* **496**, 505 (1998)
J N Abdurashitov *et al*, *Phys. Atom. Nucl.* **63**, 943 (2000)
M Cribier *et al*, *Nucl. Phys. Proc. Suppl.* **70**, 284 (1999)
S Fukuda *et al*, *Phys. Rev. Lett.* **86**, 5651 (2001)
S Fukuda *et al*, *Phys. Rev. Lett.* **86**, 5656 (2001)
Q R Ahmad *et al*, *Phys. Rev. Lett.* **87**, 071301 (2001)
[3] S Fukuda *et al*, *Phys. Rev. Lett.* **85**, 3999 (2000)
W W M Allison *et al*, *Phys. Lett.* **B449**, 137 (1999)
M Ambrosio *et al*, *Phys. Lett.* **B517**, 59 (2001)
[4] T Araki *et al*, *Phys. Rev. Lett.* **94**, 081801 (2005)
[5] M H Ahn *et al*, *Phys. Rev.* **D74**, 072003 (2006)
P Adamson *et al*, *Phys. Rev.* **D77**, 072002 (2008)
[6] K Nakamura *et al*, *J. Phys.* **G37**, 075021 (2010)
[7] M Apollonio *et al*, *Eur. Phys. J.* **C27**, 331 (2003), hep-ex/0301017

[8] P Adamson *et al*, *Phys. Rev.* **D82**, 051102 (2010), arXiv:1006.0996 [hep-ex]
[9] M Kobayashi and T Maskawa, *Prog. Theor. Phys.* **49**, 652 (1973)
[10] W Buchmuller, R D Peccei and T Yanagida, *Ann. Rev. Nucl. Part. Sci.* **55**, 311 (2005)
[11] K Abe *et al*, *Nucl. Instrum. Methods* **A659**, 106 (2011), arXiv:1106.1238
[12] D Beavis, A Carroll, I Chiang *et al*, Long Baseline Neutrino Oscillation Experiment at the AGS (Proposal E889), 1995. Physics Design Report, BNL 52459
[13] Y Hayato, *Nucl. Phys. Proc. Suppl.* **112**, 171 (2002)
[14] GEANT3, A detector description and simulation tool, 1993, Application Software Group, Computing and Networks Division, CERN, Geneva
[15] FLUKA version 2008.3c, 2008, http://www.fluka.org/fluka.php
[16] N Abgrall *et al*, *Phys. Rev.* **C84**, 034604 (2011), arXiv:1102.0983 [hep-ex]
[17] R Wendell *et al*, *Phys. Rev.* **D81**, 092004 (2010), arXiv:1002.3471 [hep-ex]
[18] P Adamson *et al*, *Phys. Rev. Lett.* **106**, 181801 (2011), arXiv:1103.0340 [hep-ex]
[19] P Adamson *et al*, *Phys. Rev. Lett.* **107**, 181802 (2011), arXiv:1108.0015 [hep-ex]
[20] K Abe *et al*, *Phys. Rev. Lett.* **107**, 041801 (2011), arXiv:1106.2822 [hep-ex]